

CELLSNAKE : A NEW ACTIVE CONTOUR TECHNIQUE FOR CELL/FIBRE SEGMENTATION

Kangyu Pan, Anil Kokaram*

Trinity College Dublin
Electronic & Electrical Engineering Department
Ireland

Kerry Gilmore, Michael J. Higgins,
Robert Kapsa, Gordon G. Wallace

Intelligent Polymer Research Institute
University of Wollongong, Australia

ABSTRACT

Active contours are well known for object segmentation and widely adopted in various forms for biological image analysis. Most of the techniques are commonly based on object geometry but overlapping regions cause severe problems to contour propagation. In this paper, we propose a novel active contour technique (“cellsnake”) for solving this problem with an application to cell and fibre segmentation. Given that the transparency of overlapped objects is unavailable, we present a new set of contour forces derived from a-priori knowledge of cell geometry that allows the contour to deform correctly in those regions. We have combined these terms with other existing forces and we show that cellsnake gives appropriate shape estimation of the objects especially in the overlapped area in the observed images.

Index Terms— Active contour, Snake, Deformable model, Geodesic active contour, Vector field convolution

1. INTRODUCTION

The development of new tissue engineering practices for skeletal muscle is critical for the reconstruction of lost or damaged muscle. Because muscle cells are responsive to electrical stimulation, we are attempting to use electrical stimulation with conductive polymer materials to control the growth of muscle cells [1]. To assess the performance of various processes, we must measure muscle cell density quantitatively. Fig.1(a) shows a typical image (1040×1388) of both cells and fibres from these experiments. The task is to count the number of muscle cells and fibres (red objects) in the field of view. A red object is classified as a cell or fibre based on the location and amount of nuclei (blue “blobs”) inside the object. When more than one nucleus exist in the same “object” that object is a fibre, otherwise it is a single cell.

The objects are usually well separated in the images, but some appear to ‘touch’ or are overlapped. Overlap appears because we are imaging in 2D, what is essentially an arrangement of cells in 3D. Traditional AC techniques would count overlapping objects as a single one so the key is to distinguish each object even though it may overlap with other cells or fibres in the tissue.

Intuitively, the images in Fig.1 show that it is rare to have complete overlap of two objects. Hence we can use the “branches” or non-overlapped portions of each (red) region (see C,D&E of Fig.1(a)), to infer how to propagate the contour *through* the overlapped regions. The idea is associating two or more “branches”, on different sides of an overlapping area, that belong to the same fibre. What is needed therefore is to modify the behavior of traditional AC techniques by incorporating the geometric equivalent of this

intuition. Of course a few alternative active models have introduced different modules to solve similar problems, such as statistical constraints [2], primitive shape priors [3] and texture [4]. These tools, however, are based in the image domain and do not incorporate shape information in a way that will overcome overlap problems.

It turns out that a muscle fibre is developed from a group of cells that appear to have the same shape as their associated nuclei. We therefore introduce a novel deformable model, “cellsnake”, that assigns one active contour to each nuclei ‘blob’ within the same object region, then enforce each AC to deform with that same shape. The overlapping contours are then merged with certain conditions during the deformation process. Consequently, instead of fitting a single active contour to each irregular fibre object with a set of complex constraints, we can propose simpler regularizing terms derived from the patterns of cellular appearance in the observed image to enforce each active contour to deform in the shape of a cell. In this paper, we alter the VFC technique from [5] and the Geodesic model from [6] to incorporate this idea. We first present some pre-processing steps and then expose the essence of the new AC.

Pre-processing: In our images, nuclei are stained blue, and the cell body is stained red (see Fig.1(a)). As the nucleus shape is used to initialize the AC, we identify the nuclei by simple thresholding of the blue channel (value of > 40 in our pictures), then the binary image is used for initial contours. The red channel is used for contour growing, but firstly denoised using wavelet denoising from [7]. For convenience in the extraction of forces, we create a modified composite image \mathbf{I} by combining the nucleus image (blue image channel, I_n) with the cell-body image (red channel I_m) with: $\mathbf{I} = I_m + \lambda_n I_n$, where $\lambda_n = 0.1$ is the mixing weight. Fig.1(b)&(c) show the blue (I_n) and red (I_m) channels respectively from one of our images. The denoised red channel is shown as Fig.1(d) and the final composite that combines (b) and (d) is shown in (e). Initial contours are derived from (b) but propagation takes place in (e).

2. ACTIVE CONTOURS

Active contour (AC), or ‘snakes’, have been formulated within an energy minimizing framework proposed by Kass *et al.*[8]. A snake is represented by a closed parametric curve $U^t = [u_1^t, \dots, u_S^t]$, where u_s^t is the position of point s (“snaxel”) of the curve at time t . An initialized AC is refined iteratively and attracted towards the object boundary by regularizing forces derived from image data. A number of existing active models [9, 10, 11] have replaced the standard external force in [8] by a sum of other forces derived from different aspects of the image data.

AC optimization is well known but the key issue is to define the internal and external forces acting on the contour. For brevity in this

*This work was part funded by Science Foundation Ireland (SFI).

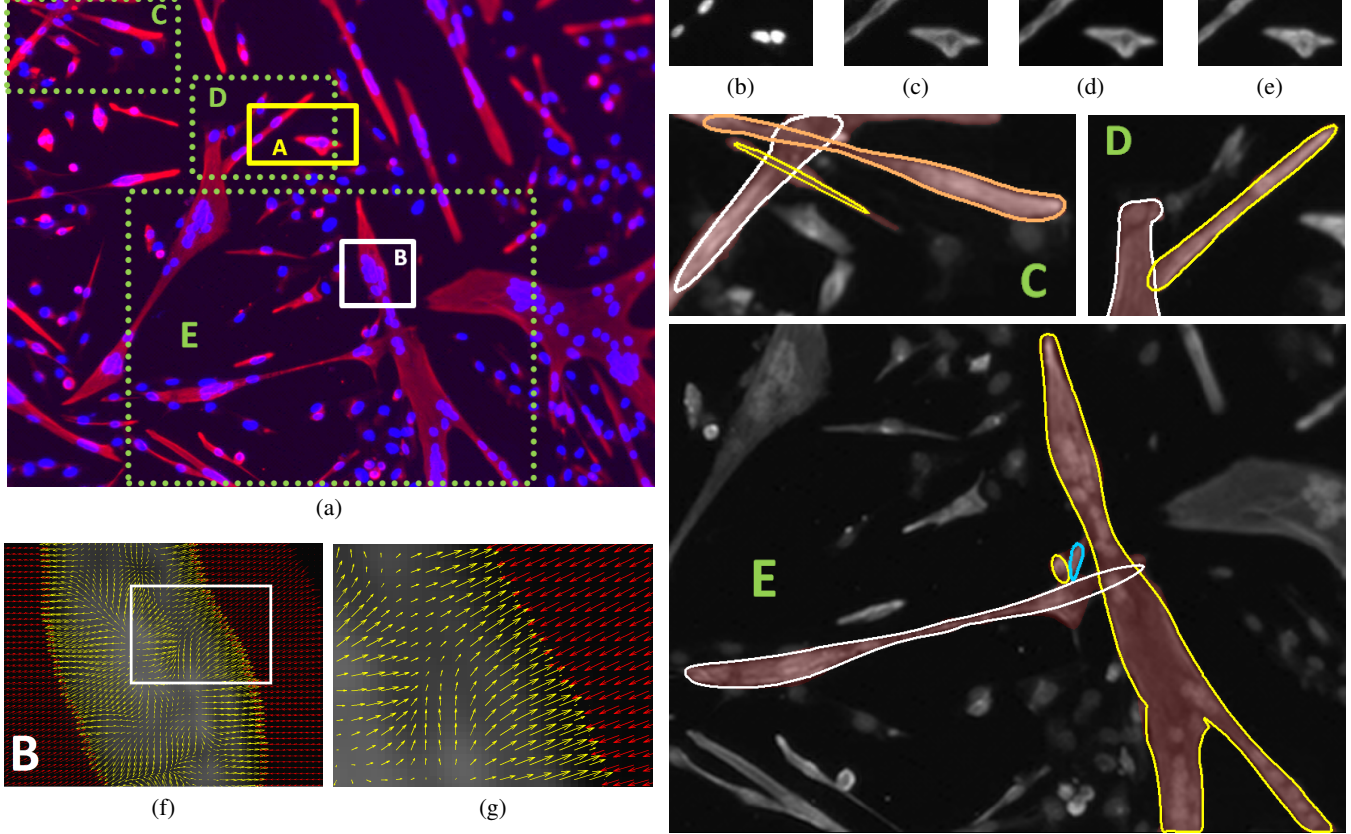


Fig. 1. Sample of skeletal cells/fibers. (a) is an image of skeletal sample that superimposes the gray scale nuclei image (blue) and cell body image (red) of muscle sample. (b) & (c) are the respective nuclei image and cell body image of region A in (a). (d) is a smoothed version of (c) after wavelet denoising. (e) is a corrected image of (d) by boosting the dimmer nuclei area. (f) displays the force field of “growth environment” of the new model in region B of (a), where the yellow arrows are f_{vfc} and the red arrows are f_b . (g) is a zoom in of the white region in (f). The bottom right images show the segmentation results, indicated by differently colored contours, for the irregular objects in region C,D&E of (a).

paper we only present our new forces from which the AC algorithm can be derived. The reader can see [5] for the actual optimization scheme we adopt. Our new forces derived from the cell specific information are combined with traditional smoothness and tauness internal forces in [8]. We also add two external forces, the VFC force f_{vfc} and the background force f_b , to the model so that the image data regulates the development of AC. Our new internal forces act like cell specific features and are discussed as a “cellular module” (f_{cell}), and the external forces form the “growth environment” (f_{vfc}, f_b). The deforming force at each snaxel is defined as $f(u_s^t) = f_{cell}(u_s^t) + k_{in}f_{vfc}(u_s^t) + k_{out}f_b(u_s^t)$ with weights $k_{in} = 1$ and $k_{out} = 1.5$. These forces are discussed next.

2.1. Environment Forces

VFC Force f_{vfc} : In order to regulate the deformation based on the image geometry, we adopt the idea of vector field convolution (VFC) proposed by Li *et al.*[5] to induce a vector field inside an object region. However Li applies this force only at object edges, but we use it here over the whole image \mathbf{I} in order to allow the cell body itself to influence the growth of the AC. The VFC induces forces that cause the contour to push from bright into darker areas and is defined as follows

$$f_{vfc}(x, y) = \mathbf{I}(x, y) * k(x, y), \quad k(x, y) = m(x, y)n(x, y) \quad (1)$$

where $k(\cdot)$ is a vector field kernel with magnitude $m(\cdot)$ and direction $n(\cdot)$ at location (x, y) . Note that $n(x, y)$ is a unit vector pointing outward from the center of the kernel at position (x, y) . In our experiments, $m(x, y)$ is a 21×21 Gaussian kernel with $\sigma = 6$.

This modified VFC can be considered as a growing environment for the active model inside the object region (yellow arrows in Fig.1(f)&(g)). However, in practice, the AC may escape beyond the cell boundary during the deformation process. To prevent this ‘leaking’ deformation, we introduce background forces f_b derived from the outside of cell (red arrows in Fig.1(f)&(g)).

Background Force f_b : Defining a cell body mask as $M_b = I_m > T_m$, ($T_m = 40$ here), the background mask is M_b in Matlab notation. f_b is derived from this background using $f_b(x) = |(G * M_b)(x)|\vec{v}_B(x)$, where G is a 7×7 Gaussian filter with $\sigma = 1.5$, and $\vec{v}_B(x)$ is a unit vector of the gradient $\vec{\nabla}(G * M_b)(x)$ at site x .

2.2. Cellular Forces

Recall that f_{cell} is designed from the pattern of cellular appearance in the observed images. We summarize the different influences with four cellular forces, $f_{cell}(u_s^t) = H\{f_e(u_s^t), f_\kappa(u_s^t), f_m(u_s^t), f_{cs}(u_s^t)\}$. Here, f_e is an elliptical weighted growing force. f_κ is a supplementary growing force based on the curvature of AC. f_m is a momentum force that includes statistical information of the iterative devel-

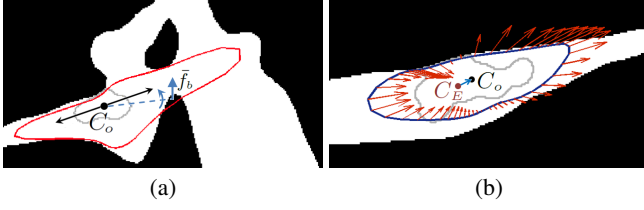


Fig. 2. Illustrations of rotational moment M_E and center shift force f_{cs} . (a) illustrates the idea of rotational moment caused by the ‘leaked’ regions. (b) shows the deformation of AC (blue curve) is constrained by f_{cs} (red arrows) derived from the center shifting between the center C_o of nuclei (gray contour) and the elliptical center C_E of AC.

oment at each snaxel, and f_{cs} is a center shift force. Since the ‘cellular module’ is invariant to image topology, we employ a level-set framework introduced by Osher *et al.*[12], to characterize the active region in order to design the cellular forces.

Elliptical Force f_e : Fig.1(a) shows that the shape of each muscle cell tends to be long and thin. We therefore propose an elliptical force f_e applied to each snaxel with different weights w_θ depending on the position of the snaxel on AC. This encourages the AC to grow along the major axis instead of the minor axis. At each iteration, the AC is fitted with an ellipse in order to find the major and minor axes, d_{E1} and d_{E2} , and the elliptical orientation angle θ_E . Then given the orientation angle $\theta_e(u_s^t)$ of $f_e(u_s^t)$ on snaxel s at time t , the corresponding $w_\theta(u_s^t)$ is estimated by

$$w_\theta(u_s^t) = \frac{\cos(2(\theta_e(u_s^t) - \theta_E(t))) + 1}{2} \frac{d_{E1}(t) - d_{E2}(t)}{d_{E1}(t)} + \frac{d_{E2}(t)}{d_{E1}(t)} \quad (2)$$

The direction of the elliptical force described by $\vec{v}_e(u_s^t) = \lambda_1 \vec{v}_c(u_s^t) + \lambda_2 \vec{n}_\phi(u_s^t)$. Where $\vec{v}_c(u_s^t)$ is a unit vector from the nuclei center C_o of AC to snaxel s , $\vec{n}_\phi(u_s^t)$ is the unit normal vector of AC at snaxel s , and $\{\lambda_1, \lambda_2\}$ are coefficients that $\lambda_1 + \lambda_2 = 1$. The elliptical force is then defined as $f_e(u_s^t) = w_\theta(u_s^t) \vec{v}_e(u_s^t)$

Rotational Moment - Fig.2(a) shows an AC leaking slightly into a black background region in the area of overlap. Normally, the background force would prevent this, but in this case due to the finite number of snaxels, there is no snaxel at the leakage point in the contour. When that happens, even though the background force could help, there is no snaxel to ‘take the hint’. To solve this problem we must somehow move the existing snaxels which may be elsewhere, in such a way as to respond to this ‘leakage’. The background force f_b in the ‘leaked’ region, shown by a blue arrow in the figure, is therefore used to rotate the elliptical orientation angle θ_E of the whole contour. We derive a rotational moment M_E , from the mean background force $\bar{f}_b(l)$ of each ‘leaked’ region l with area size $A(l)$. Given L ‘leaked’ regions, the adjusted elliptical rotation angle θ_E^* is as follows

$$\theta_E^*(t) = \theta_E(t) + \frac{1}{e_\theta} \sum_{l=1}^{L(t)} A(l) M_E(l), \quad M_E(l) = \bar{f}_b(l) \sin(\theta_{\bar{f}_b}(l) - \theta_c(l)) \quad (3)$$

where e_θ is a regularizing factor, $\theta_{\bar{f}_b}$ is the orientation angle of \bar{f}_b and $\theta_c(l)$ is the orientation of the center of l related to the center C_o of AC. This new orientation θ_E^* then replaces θ_E in Eq.(2) and hence the evolution of all of the snaxels is affected subtly to reduce the leakage and lead to a better shape estimation of corresponding overlapping object.

Force Deflection - As shown in Fig.3(a), the inactive snaxels (with growing directions close to the minor axis) become stationary when reaching the boundary of an object region. Due to smoothness

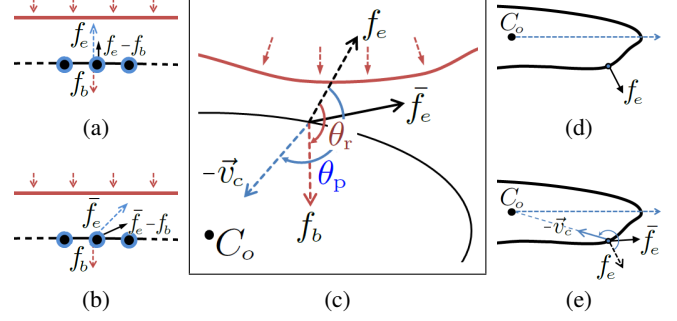


Fig. 3. Force deflection. (a) shows the inactive snaxels that are ‘trapped’ at the edge of object region. (b) illustrates the idea of repulsive force deflection for solving the ‘trapped’ problem in (a). (d) shows an unwanted deformation of AC due to divergence of growing directions. (e) illustrates the idea of pulling force deflection for reducing the divergence in (d). (c) shows the overall force deflection to the cellular elliptical force.

and rigidity effects of internal forces, these snaxels cause unwanted restriction to the overall development of AC. The solution is to force these snaxels to move along the object boundary rather than being ‘trapped’ at the boundary. To do so we introduce a ‘repulsive’ force deflection (Fig.3(b)) to the major growing force $f_e(u_s^t)$. The idea is, as illustrated in Fig.3(c), to alter $\theta_e(u_s^t)$ by the angular difference $\theta_r(u_s^t)$ between $f_e(u_s^t)$ and the background force $f_b(u_s^t)$.

In addition, (see Fig.3(d)), an unwanted divergence of growing directions of snaxels (related to the major axis) can be induced by the ‘environment’ forces in the ‘overlapping’ area of object region. To prevent this we propose another force deflection to $f_e(u_s^t)$ by assuming C_o has a pulling effect on the contour (Fig.3(e)). The pulling deflection is an alteration of $\theta_e(u_s^t)$ using the angular difference $\theta_p(u_s^t)$ between $f_e(u_s^t)$ and the vector $-\vec{v}_c(u_s^t)$.

By regulating the repulsive and pulling deflections with weights λ_p and λ_r respectively, the orientation angle $\bar{\theta}_e(u_s^t)$ of deflected elliptical force $\bar{f}_e(u_s^t)$ is estimated by

$$\bar{\theta}_e(u_s^t) = \theta_e(u_s^t) + \lambda_p \theta_p(u_s^t) + \lambda_r \theta_r(u_s^t) \quad (4)$$

And therefore $\bar{f}_e(u_s^t) = |f_e(u_s^t)| \angle \bar{\theta}_e(u_s^t)$.

Curvature Force f_κ : As stated previously, object regions tend to be narrow in the un-overlapped areas. An AC should progress quickly through such narrow areas in order to deform with the same shape. However, the weak object information in the narrow area induces a weak inner environment force f_{vc} and stronger outer environment force f_b , and hence results in slow development. Since an AC has higher curvature in the narrower area, we apply a curvature force f_κ to overcome this. Similar to the applications of curvature in [9, 4], f_κ for each snaxel is defined as $f_\kappa(u_s^t) = \kappa(u_s^t) \vec{n}_\phi(u_s^t)$, where $\kappa(u_s^t) = \text{div} \left(\frac{(\nabla U_s)^t}{|(\nabla U_s)^t|} \right) (u_s^t)$ is the curvature value of AC at u_s^t .

Momentum Force f_m : In order to inject an ‘evolution memory’ to the AC model, we propose f_m derived from the correlation between the present deformation at t and the previous deformation at $t - 1$. The idea is to smooth out noise in the displacement of each snaxel over the evolution of the contour. f_m is therefore a deformation momentum at each snaxel, and is defined as

$$f_m(u_s^t) = \left(\vec{v}_e(u_s^t) \cdot \left(\frac{u_s^t - u_s^{t-1}}{|u_s^t - u_s^{t-1}|} \right) \right) \vec{v}_e(u_s^t) \quad (5)$$

As f_e is a major ‘growing’ force of our active model and usually dominate the deformation of active contour, the direction $\vec{v}_e(u_s^t)$ can then be considered as the current growing direction of AC at u_s^t .

Center Shift Force f_{cs} : It is important to enforce the constraint that the nucleus of each cell is generally near the centre of mass of the cell. A center shifting constraint is therefore induced to the AC in terms of a cellular force f_{cs} . As illustrated in Fig.2(b), $f_{cs}(u_s^t)$ at each snaxel is an attractive or repulsive force derived from the displacement from elliptical center C_E^t of AC at time t to the center C_o of nuclei region (the initial AC). Hence f_{cs} is defined as

$$f_{cs}(u_s^t) = -k_{cs}(u_s^t)\vec{v}_c(u_s^t), \quad k_{cs}(u_s^t) = \frac{D_{Eo}^t}{\bar{D}_{so}^t} \cos(\theta_c(u_s^t) - \theta_{Eo}^t) \quad (6)$$

where D_{Eo}^t is the distance, with orientation θ_{Eo}^t , from C_E^t to C_o , \bar{D}_{so}^t is the mean distance from snaxels to C_o , and θ_c is the orientation angle of \vec{v}_c .

Final Expressions: The ‘cellular module’ $f_{cell}(u_s^t)$ is finally expressed as

$$f_{cell}(\cdot) = g(u_s^t)(d_s^t(w_e \bar{f}_e(\cdot) + w_\kappa f_\kappa(\cdot) + w_m f_m(\cdot)) + w_{cs} f_{cs}(\cdot))$$

where $\{w_e, w_\kappa, w_m, w_{cs}\}$ are the mixing coefficients and assigned respectively with the values $\{5, 2, 1, 5\}$ in our experiments. g is a Geodesic factor proposed by Caselles *et al.* in [6] that is derived from the image gradient of \mathbf{I} , and defined as $g(u_s^t) = \frac{1}{1+|\nabla \mathbf{I}(u_s^t)|^\gamma}$ with a regulating factor $\gamma = 2$. We use g to reduce the cellular forces near to object boundaries, in order to prevent ‘leakage’.

To prevent contours growing too large, d_s is a growing rate factor that reduces the effect if the environment and center shift forces as the area of the AC increases. d_s is designed as follows:

$$d_s^t = \begin{cases} \exp(-\gamma_s \frac{A_{ac}(t) - \bar{A}_{cell}}{\bar{A}_{cell}}) & , A_{ac} < \bar{A}_{cell} \\ 1 & , A_{ac} \geq \bar{A}_{cell} \end{cases}$$

where $A_{ac}(t)$ is the area inside AC at time t , γ_s is a constant regulating factor and \bar{A}_{cell} is an area threshold. d_s

It is clear that the end of this process will result in the same number of ACs as nuclei. Hence, as a final step in order to fit the fibre objects all overlapping ACs are merged. Our merge conditions as follows

- if $\frac{A_{ab}}{A_a} > T_{A_{max}}$ or $\frac{A_{ab}}{A_b} > T_{A_{max}}$
- if $\frac{A_{ab}}{A_a} > T_{A_{min}}$ or $\frac{A_{ab}}{A_b} > T_{A_{min}}$, and $\cos(\theta_{ea} - \theta_{eb}) < T_\theta$

where A_{ab} is the overlapped area, A_a and A_b are the area of active contours U_a^t and U_b^t respectively, θ_{ea} and θ_{eb} are the elliptical orientation angles of a and b respectively. Note $T_{A_{max}}$, $T_{A_{min}}$ and T_θ are user defined thresholds, and are assigned respectively with values 0.6, 0.1 and 0.7 in our experiments.

3. RESULTS AND CONCLUSION

As shown in Fig.1, our active model has successfully segmented the joined/overlapped fibers, and also gives appropriate shape estimate for the objects in the overlapping area. That figure does not show the other fibres which were segmented since there was no overlap in these other areas in this portion. In order to achieve optimum segmenting results, the AC model requires slightly different weights depending on the complexity of the object regions in different images. The reader is directed to <http://www.mee.tcd.ie/~sigmedia/Research/ICIP11Cellsnake> for movies of contour evolution for different images and a visual comparison with standard AC techniques in this context. The principal reason why the process works here is because of the appropriate constraints that were used for the shapes in these images. Furthermore, our

deflection force solves a well known problem in AC work i.e. that contour evolution tends to slow down entirely when some portion of the contour gets near to a boundary. However our shape implicit forces can be used to constrain contour evolution for other image content simply by replacing the elliptical model in Eq.(2) with the appropriate shape mode. Computational load is proportional to the number of snaxels on a contour, and the number of contours used in an image. Our implementation is quite inefficient in Matlab, taking about 2hrs for the example shown which used 100 iterations and a maximum displacement at each snaxel of 12 pixels, but this can be improved substantially by parallelization (each contour can evolve within its own processing thread). In each contour iteration step the main computational modules are i) calculating the elliptical model and ii) calculating deflection and curvature forces. Even so the computational load per snaxel is relatively low since the Environment forces can be pre-calculated and the remaining load is principally angle calculations. The remaining problems to be solved are automating the calculation of the regulating coefficients and mixing weights of the cellsnake model for ‘‘weak’’ (dimmer and narrower) objects overlapping in different situations. We are currently addressing this as an adaptive process.

4. REFERENCES

- [1] K. J. Gilmore, M. Kita, Y. Han, A. Gelmi, M. J. Higgins, S. E. Moulton, G. M. Clark, R. Kapsa, and G. G. Wallace, ‘‘Skeletal muscle cell proliferation and differentiation on polypyrrole substrates doped with extracellular matrix components’’, *Biomaterials*, vol. 30, pp. 589–601, 2009.
- [2] I. Ben Ayed, S. Li, and I. Ross, ‘‘Level set image segmentation with a statistical overlap constraint’’, *IPMI 2009, LNCS 5636*, pp. 589–601, 2009.
- [3] A. K. Hamou and M. R. El-Sakka, ‘‘Optical flow active contours with primitive shape priors for echocardiography’’, *EURASIP Journal on Advances in Signal Processing*, 2010.
- [4] M. Alemán-Flores, L. Álvarez, and V. Caselles, ‘‘Texture-oriented anisotropic filtering and geodesic active contours in breast tumor ultrasound segmentation’’, *Journal of Mathematical Imaging and Vision*, vol. 28, no. 1, pp. 81–97, 2007.
- [5] B. Li and S. T. Acton, ‘‘Active contour external force using vector field convolution for image segmentation’’, *IEEE Transactions on Image Processing*, vol. 16, no. 8, pp. 2096–2106, 2007.
- [6] V. Caselles, R. Kimmel, and G. Sapiro, ‘‘Geodesic active contours’’, *Proc. of 5th ICCV*, pp. 694–699, 1995.
- [7] A. Baradarani and R. Yu, ‘‘A dual-tree complex wavelet with application in image denoising’’, *Proc. of ICIP 2007*, pp. 1203–1206, 2007.
- [8] M. Kass, A. Witkin, and D. Terzopoulos, ‘‘Active contour models’’, *Proc. of 1st ICCV*, pp. 259–268, 1987.
- [9] T. F. Chan and L. A. Vese, ‘‘Active contours without edges’’, *IEEE Transactions on Image Processing*, vol. 10, no. 2, pp. 266–277, 2001.
- [10] G. S. Muralidhar, A. C. Bovik, J. D. Giese, M. P. Sampat, G. J. Whitman, T. M. Haygood, T. W. Stephens, and M. K. Markey, ‘‘Snakules: A model-based active contour algorithm for the annotation of spicules on mammography’’, *IEEE Transactions on Medical Imaging*, vol. 29, no. 10, pp. 1768–1780, 2010.
- [11] M. S. Kulikova, I. H. Jermyn, X. Descombes, E. Zhizhina, and J. Zerubia, ‘‘Extraction of arbitrarily-shaped objects using stochastic multiple birth-and-death dynamics and active contours’’, *SPIE-IS&T Electronic Imaging*, vol. 7533, 2010.
- [12] S. Osher and J. A. Sethian, ‘‘Fronts propagating with curvature dependent speed: Algorithms based on hamilton-jacobi formulations’’, *Journal of Computational Physics*, vol. 79, pp. 2096–2106, 2007.